JOURNAL OF GEOPHYSICAL RESEARCH, VOL. 113, E07010, doi:10.1029/2007JE003047, 2008

Dust charging and electrical conductivity in the day and nighttime atmosphere of Mars

M. Michael,[1] S. N. Tripathi,[1] and S. K. Mishra[1]

Received 24 November 2007; revised 18 January 2008; accepted 17 March 2008; published 19 July 2008.

[1] Understanding aerosol charging and atmospheric conductivity are necessary in describing the global electric circuit, the aerosol coagulation rate, aerosol-cloud interaction and their subsequent affect on the climate. The importance of aerosol charging for the conductivity variations of the lower Martian atmosphere during both day and night is calculated. Galactic cosmic rays are the dominant ionizing agent in the lower atmosphere, producing molecular ions and ion clusters. During the nighttime these ion clusters get attached to the aerosols and charging occurs. Solar UV photons are an additional ionizing agent during the day-time. Only solar photons of energy less than 6 eV reach the surface of Mars as those with energies greater than 6 eV are absorbed by atmospheric molecules before they reach the lower atmosphere. Those photons which do reach the lower atmosphere ionize the aerosols as the ionization potential of most of the aerosols is less than 6 eV and produce electrons. Aerosols become charged by the attachment of ions and electrons during the day-time. The ion-aerosol and electron-aerosol attachment coefficients, as well as the ion-ion and ion-electron recombination rates are calculated. The charge distribution of aerosols is obtained by the simultaneous solution of the ion-aerosol charge balance equations. Both the steady state and time dependent concentration of charged aerosols are calculated. More than 60% of the ions and 95% of the electrons get attached to the aerosols. There are more negatively charged aerosols in steady state due to the presence of highly mobile electrons during the day-time. The presence of electrons increases the conductivity during the day time. The day-time results are compared with the nighttime results.

Citation: Michael, M., S. N. Tripathi, and S. K. Mishra (2008), Dust charging and electrical conductivity in the day and nighttime atmosphere of Mars, *J. Geophys. Res.*, *113*, E07010, doi:10.1029/2007JE003047.

1. Introduction

[2] The atmosphere of Mars always has a thin veil of dust particles suspended in the air. The amount of dust in the atmosphere varies significantly with season, with a minimum during northern summer (optical depth $\sim$ 0.1–0.3) and maximum during northern winter (optical depth $\sim$ 2–5) [*Read and Lewis*, 2004]. The behavior of dust and its long-range transport during dust-storms within the atmosphere are major components of the atmospheric environment and climate system on Mars.

[3] These dust particles can be electrically charged by various mechanisms [*Melnik and Parrot*, 1998] which is important for a number of reasons. Electrical charging reduces the aerosol coagulation rate. The lower coagulation rate increases the settling time of the aerosols and thereby increases aerosol concentrations that in turn affect the optical depth of the atmosphere and hence the atmospheric structure. The charging of aerosols enhances the aerosol-cloud interactions and ice nucleation, and reduces the conductivity of the atmosphere by reducing the mobility of the charge carriers. Knowledge of atmospheric conductivity is very important in understanding the global electric circuit of the Martian atmosphere. A constant current generator and a finitely conducting atmosphere are essential for the existence of a global electric circuit in an atmosphere. *Farrell et al.* [1999] modeled the possible electrification of Martian dust storms based on the effective electrical charging of an individual dust grain. *Farrell and Desch* [2001] have suggested that Mars possesses a global electric circuit driven by dust storms. Therefore the altitude profile of the conductivity of the atmosphere discussed in the present work will be valuable in the investigation of the global electrical circuit in the Martian atmosphere.

[4] *Melnik and Parrot* [1998] modeled the occurrence of electrical discharge in the large dust storms on Mars. It was shown that the breakdown electric field is lower in the Martian atmosphere than on Earth and breakdown can occur under certain conditions prevailing in the Martian atmosphere [*Melnik and Parrot*, 1998]. *Krauss et al.* [2006] studied in detail the electrostatic discharges on Mars. Turbulent motions within a dust storm cause dust grains to come into contact with one another. When two particles

[1]Department of Civil Engineering, Indian Institute of Technology, Kanpur, India.

0148-0227/08/2007JE003047$09.00

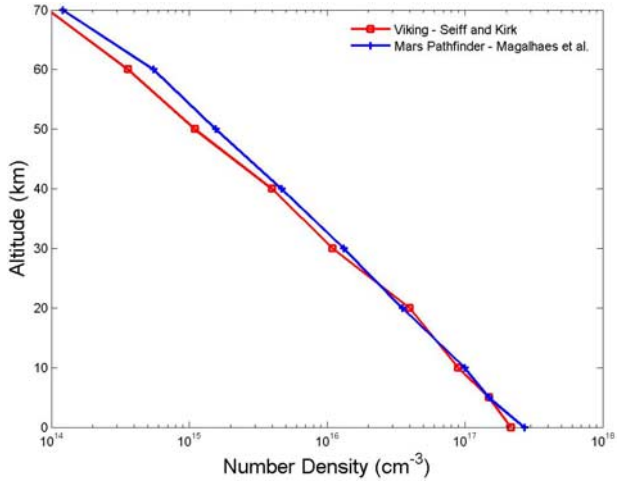

Figure 1. Atmospheric density in the atmosphere of Mars reported by *Seiff and Kirk* [1977], and *Magalhaes et al.* [1999].

of identical composition collide, the particle with the larger radius preferentially becomes positively charged. Upwinds during dust storms cause smaller negatively charged particles to be lifted to higher altitudes while larger, positively charged particles remain closer to the surface. This charge separation causes the formation of an electric field. The strength of the electric field depends on the dust density and the amount of charge generated on each grain. When the electric field within the dust cloud exceeds the breakdown electric field of the surrounding atmosphere, the charge is released in a discharge similar to lightning. Theory, laboratory experiments, and field measurements on Earth suggest that the electrically charged Martian dust storms are potential hazards to Landers. The development of a large-scale electric field on Mars is important for the transport of dust particles, since for micron size particles electrical forces may become comparable to the drag forces, and surface material chemistry etc.

[5] As none of the missions to Mars included electrical instrumentation, the only experimental evidence for electrical activity is the electrostatic adhesion of dust to the wheels of the Mars Pathfinder and Sojourner rovers [*Ferguson et al.*, 1999]. Most of the previous studies of the charging mechanisms operating in the Martian atmosphere are focused on aerosols close to the surface. The present work calculates the aerosol charging for altitudes from 0 to 70 km. *Michael et al.* [2007] have recently studied the aerosol charging and conductivity during the nighttime lower atmosphere and discussed the major results of the study. The present work concentrates more on the day time calculations and comparison with the nighttime results.

[6] Charging of aerosols occurs by the attachment of ions and electrons. As discussed by *Yair and Levin* [1989], charge balance equations can be used to calculate the steady state ion and electron concentrations and aerosol charge state. These equations are solved to obtain steady state concentrations of positive and negative ions, electrons and charged aerosol particles. A similar procedure was recently used by *Borucki et al.* [2006] and *Whitten et al.* [2007, 2008] to calculate the electrical conductivity and charging of aerosols in the atmosphere of Titan and Jupiter. The atmospheric environment, aerosol characteristics, ion and electron production rates, ion-ion and ion-electron recombination coefficients and ion-aerosol and electron-aerosol attachment coefficients are described in the following sections. These are used to calculate ion and aerosol concentrations and the conductivity of the lower atmosphere of Mars.

2. Atmospheric Environment

[7] The spacecraft Mars 6 obtained the first in situ measurements of the atmospheric structure during its entry into the Martian atmosphere in 1974 [*Kerzhanovich*, 1977], confirming remote sensing observations of a 5.45 mbar surface pressure. The Atmosphere Structure Experiment on the two 1976 Viking landers [cf. *Seiff*, 1976] provided the first high vertical resolution profiles of temperature, pressure, and density from the surface to 120 km [*Seiff and Kirk*, 1977]. The altitude profiles of density and temperature from *Seiff and Kirk* [1977] are provided in Figures 1 and 2, respectively. There were no spacecraft observations until Mars Pathfinder landed in July 1997, within 850 km of the Viking 1 landing site in the northern summer. The Mars Pathfinder atmospheric structure investigation (ASI) accelerometer data had improved sensitivity and higher digital resolution compared to the data from the Viking missions [*Magalhaes et al.*, 1999]. The atmospheric density and temperature observed by the Pathfinder ASI accelerometer is presented in Figures 1 and 2, respectively. The number density for altitudes less than 70 km is in good agreement with the Viking 2 observations and is used in the present study.

[8] *Hinson et al.* [2004] have discussed the profiles of temperature obtained from the Thermal Emission Spectrometer (TES) and the Radio Science (RS) experiment onboard Mars Global Surveyor. These observations were made in the latitudes of 62°–85°N during midspring to early autumn. The zonally averaged temperature profiles

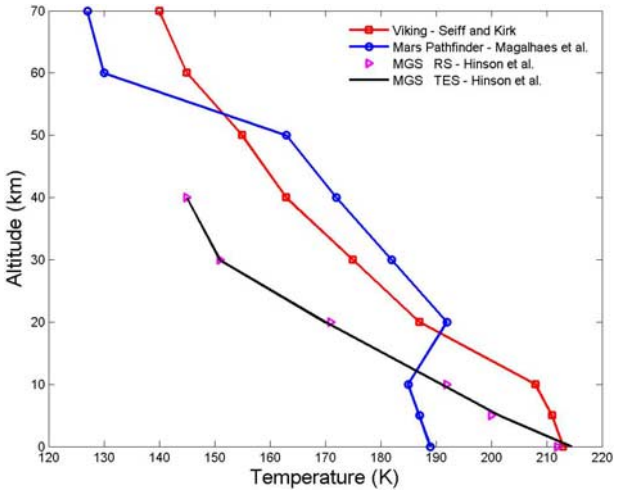

Figure 2. Temperature structure of the atmosphere of Mars reported by *Seiff and Kirk* [1977], *Magalhaes et al.* [1999], and Mars Global Surveyor RS and TES observations from *Hinson et al.* [2004].

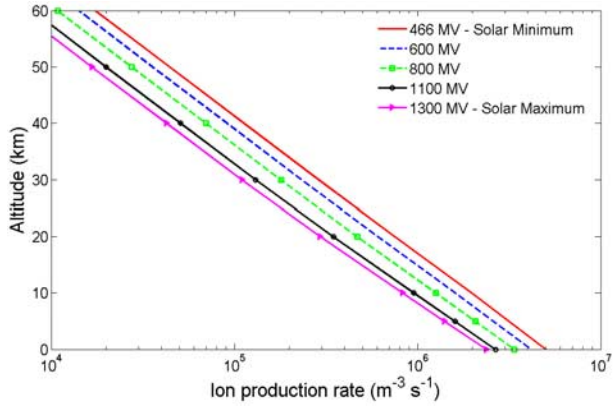

Figure 3. Ion production rates for various solar activities.

from RS and TES are presented in Figure 2. Though Mars Express, Mars Odyssey and Mars Reconnaissance Orbiter have been collecting excellent data, none of the publications include profiles of atmospheric density and temperature for the altitudes of interest of the present work.

3. Ion Production

[9] Ionization rates are required to calculate the ion concentrations and, therefore, it is essential to consider the various ionization processes. *Whitten et al.* [1971] carried out a detailed study of the lower ionosphere of Mars, considering ionization by galactic cosmic rays (GCR) and solar radiation in an ion-neutral model and calculating the concentration of ions and electrons below 80 km. *Molina-Cuberos et al.* [2001] improved the study of the lower ionosphere of Mars by developing a more detailed ion-neutral model which includes more neutral compounds and reaction rates than previous studies. *Molina-Cuberos et al.* [2001] have calculated the GCR ionization rates of CO_2, N_2 and Ar. GCR come from interstellar medium and as they approach the Sun they encounter the solar wind and the magnetic field associated with it. As a result, the GCR lose some of their energy and many do not reach Earth (or Mars). In times of higher solar activity this effect is stronger and fewer cosmic rays reach the Earth or Mars. Therefore GCR flux is minimum during the period of maximum solar activity. The ionization by GCR in the Martian atmosphere is mainly due to the slowing down of protons and *Molina-Cuberos et al.* [2001] have used measurements of the dissociative and nondissociative ionization of CO_2 and N_2 by proton impact. The maximum ion concentration occurs at the surface. Hydrated hydronium ions $H_3O^+(H_2O)_n$ (n, varies from 1 to 4) are the most abundant positive ions for all altitudes below 70 km. $CO_2^+CO_2$ becomes important at altitudes more than 65 km. The most abundant negative ion is $CO_3^-(H_2O)_2$. In the present study the most abundant positive ion considered is $H_3O^+(H_2O)_4$ and the most abundant negative ion is $CO_3^-(H_2O)_2$.

[10] *O'Brien* [1970] developed an analytical theory of the transport of GCR through the Earth's atmosphere and the predictions of this model agree very well with the experimental measurements of the particle fluxes at different longitudes and magnetic conditions [*Boella et al.*, 1968; *Roesler et al.*, 1998; *Molina-Cuberos et al.*, 1999]. The same model has been applied to find the particle flux at Mars. O'Brien (private communication) calculated the ion production rates at different altitudes in the Mars atmosphere corresponding to different solar activities. The ion production rates for heliocentric potential 466, 500, 600, 800, 900, 1000, 1100, 1200, and 1300 MV are calculated and a few of these are presented in Figure 3. The heliocentric potentials 466 MV and 1300 MV correspond to the minimum and maximum solar activities, respectively.

4. Aerosol Characteristics

[11] The size of the dust particles in the Martian atmosphere has been known since Mariner 9 and Viking missions [*Conrath*, 1975; *Pang and Ajello*, 1977; *Toon et al.*, 1977]. Observations of Martian aerosols from Viking orbiter and Lander cameras are discussed by *Clancy and Lee* [1991] and *Pollack et al.* [1979]. *Clancy and Lee* [1991] suggested that the effective radius of the dust particles, as seen from the Martian surface, is $\sim$2.5 μm and the size distribution of dust is constant at subsolar latitudes. *Murphy et al.* [1993] have compiled all the results obtained from spacecraft observations up to the Viking mission and developed a zonally symmetric numerical model for aerosol transport. Later the vertical profiles of the mixing ratio and size of the dust particles in the 15–25 km altitude range were estimated from the solar occultation measurements performed by the Auguste instrument onboard Phobos 2 spacecraft [*Korablev et al.*, 1993; *Chassefiere et al.*, 1992]. The measurements were made in the equatorial region near the northern spring equinox. The effective radius of the particles was found to be $\sim$0.8 μm at 25 km and $\sim$1.6 μm at 15 km. Their number density is $\sim$0.3 cm^{-3} in the same altitude range and the effective variance of the distribution is $\sim$0.25. An effective radius of $\sim$1.25 μm was inferred from the analysis of the dust component observed by the ISM infrared spectrometer [*Drossart et al.*, 1991].

[12] *Chassefiere et al.* [1995] reanalyzed the phobos results to obtain a consistent outlook. The solar occultation measurements provided the vertical structure of the dust in the 15–25 km altitude region and the infrared imaging characterized the dust particles in the lower altitudes. These two measurements were merged to obtain the vertical dust profile from the surface to an altitude of 25 km. The similarity between the vertical profiles of dust extinction coefficient obtained by solar occultation at various longitudes showed that atmospheric conditions do not change much in space and time at these low latitudes during the early northern spring period. *Chassefiere et al.* [1995] have extrapolated the solar occultation profiles from the 15–25 km altitude range down to the ground by using a specific parameterization of the altitude dependence of the volume of particles per unit atmospheric volume and the particle effective radius. The parameterization procedure is based on the simplified steady state model used by *Chassefiere et al.* [1992]. The extrapolated quantities are then compared to those observed by the infrared spectrometer. In view of all the observations by Phobos, *Chassefiere et al.* [1995] have estimated the variance in the effective radius to be 0.25. Considering the uncertainties in the observed data, *Chassefiere et al.* [1995] have developed two more altitude profiles of aerosol concentration and effective radius

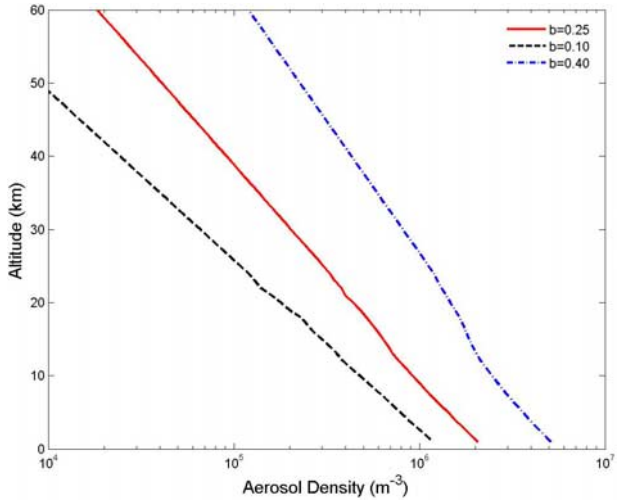

Figure 4. Aerosol density in the atmosphere [*Chassefiere et al.*, 1995].

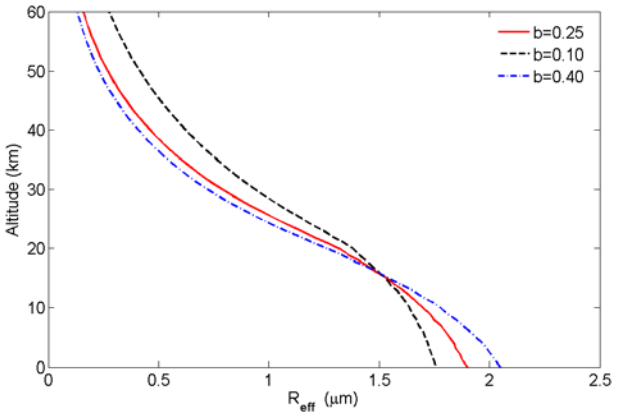

Figure 5. Effective radius of the aerosols in the atmosphere [*Chassefiere et al.*, 1995].

corresponding to maximum (0.4) and minimum (0.1) effective variances. All the three altitude profiles of the concentration and effective radius of aerosols, which are used in the present study, are presented in Figures 4 and 5.

[13] Mars aerosol studies with the Mars Global Surveyor Thermal Emission Spectrometer during 1999-2001 have been reviewed by *Clancy et al.* [2003]. They suggested that the dust particle sizes vary with respect to latitudes. The vertical structure of these variations is not available and have not been included in the present model. *Montmessin et al.* [2006] presented the aerosol size distribution from the SPICAM ultraviolet instrument onboard Mars Express. It was found that the UV measurements for aerosol particle size for altitudes greater than 55 km agree with the profile used in the present study, but for altitudes less than 55 km the size distribution obtained from the UV instrument is not consistent.

5. Solar UV Interaction and Electron Production

[14] *Grard* [1995] reported on the solar photon interaction with the lower atmosphere of Mars. Those solar photons which reach the lower atmosphere of Mars are represented by energies which are too small to ionize any of the gaseous constituents in the atmosphere. Solar UV photons of energy greater than 6 eV are absorbed by atmospheric molecules in the ionosphere. *Grard* [1995] estimated that the particles in the lower atmosphere have a wok function less than 6 eV and therefore photoelectrons can be emitted. According to *Grard* [1995] the emitted photoelectrons have a mean kinetic energy which is 3 times less than that in space and a flux which is 100 times less than it would be in the absence of any atmosphere. Solar photons incident on the Martian atmosphere are obtained by scaling the measurements performed at the Earth orbit [*Kuhn and Atreya*, 1979].

[15] A flow diagram of the solar UV interaction and the production of electrons is presented in Figure 6. The solar radiation that reaches the upper boundary (70 km) is attenuated by the absorption and scattering of aerosols in the atmosphere. The photon flux with energies less than 6 eV were obtained from *Grard* [1995]. The absorption and scattering cross sections were calculated by using a Mie code [*Dave*, 1968] for a given size parameter and refractive index. The code cites the algorithm in which the Helmholtz equation is solved in the spherical coordinate system. Incident and scattered electric and magnetic fields are expressed in terms of suitable vector spherical functions which work as a basis to expand the field space. The expanded fields satisfy the divergence-free and radiation condition. The unknown coefficients used in expansion of fields are computed using tangential boundary conditions. The numerical value of the field expansion coefficients leads to the optical properties of the spherical particle. The major inputs for the Mie code are the size parameters and the refractive index (the real and imaginary parts are 1.4 and 0.04 respectively) of the dust particles [*Chassefiere et al.*, 1995]. The size parameter depends on the effective radius [*Chassefiere et al.*, 1995] of the particle and the wavelength used. The size parameter varies from about 1 to 50 between the two boundaries (70–0 km). The extinction cross section is higher for particles of larger size parameter

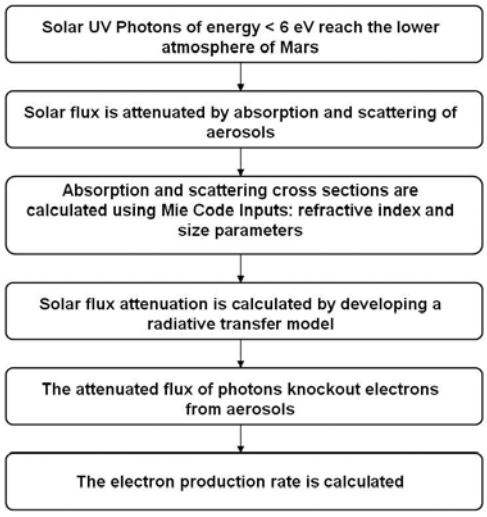

Figure 6. Flow diagram of the photoelectron production by the interaction of solar UV radiation with aerosols.

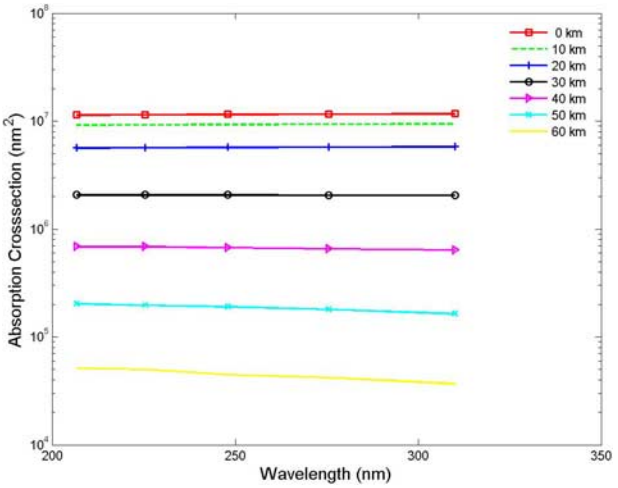

Figure 7. Crosssection of absorption of solar UV radiation by aerosols.

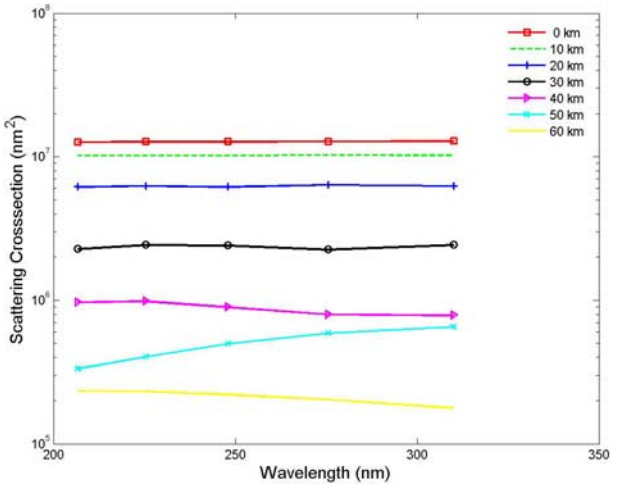

Figure 8. Crosssection of scattering of solar UV radiation by aerosols.

and thus the absorption and scattering cross sections are higher at lower altitudes where the radius of the particles are larger. As the aerosols have a work function of about 4 eV [*Grard*, 1995], the solar photons of energy between 4 to 6 eV (~206–310 nm) are considered. Figure 7 presents the photon absorption cross section by aerosols and Figure 8 depicts the scattering cross section at different altitudes. Absorption and scattering cross sections are functions of particle size; the cross sections decrease as the size of the aerosol decreases, i.e., the cross sections decrease as the altitude increases.

[16] The attenuation of the solar photons in the atmosphere is then calculated using a two-stream radiative transfer model in which the radiation directions are either downward or upward via backscattering. The equations used are the following [*Banks and Kockarts*, 1973].

$$\frac{d\Phi^+(z,\lambda)}{dz} + (\sigma_{ext})N(z)\Phi^+(z,\lambda) = N(z)\sigma_{scat}\Phi^-(z,\lambda) \quad (1)$$

$$\frac{d\Phi^-(z,\lambda)}{dz} - (\sigma_{ext})N(z)\Phi^-(z,\lambda) = -N(z)\sigma_{scat}\Phi^+(z,\lambda) \quad (2)$$

Here σ_{ext} is the sum of the absorption and scattering cross sections and σ_{scat} is the scattering cross section of aerosols, N(z) is the number density of the aerosols, $\Phi^+(z, \lambda)$ and $\Phi^-(z, \lambda)$ are, respectively, the downward and upward (scattered) solar ultraviolet intensities as functions of altitude and wavelength. The boundary conditions are: Φ^+ is the unattenuated intensity at the upper boundary and Φ^- is zero at the planetary surface [*Kuhn and Atreya*, 1979; *Borucki et al.*, 2006]. The computations are initiated by assuming that $\Phi^- = 0$ at all altitudes.

[17] The photoelectron production rate is then calculated as

$$q_e = \int_{\lambda\min}^{\lambda\max} W(z,\lambda)\sigma_x(\lambda)d\lambda \quad (3)$$

Here $W(z, \lambda)$ is the attenuated solar flux (the sum of $\Phi^+(z, \lambda)$ and $\Phi^-(z, \lambda)$) at each altitude for each wavelength. σ_x is the cross section for the photo-production of electrons by aerosols. λ_{min} and λ_{max} provide the wavelength range (206 to 310 nm) from the short wavelength cut off to the longest wavelength that produces photo-ionization. σ_x is approximated as two orders of magnitude less than absorption cross section analogous to the ionization cross-section of molecules. The work function for the aerosols to produce ionization in the atmosphere of Mars is ~4 eV [*Grard*, 1995]. As mentioned above, all the solar photons of energy greater than 6 eV are absorbed in the ionosphere and those of energy less than 4 eV are not able to knock out electrons from particles. Therefore photoelectrons are produced only when solar photons of energy 4–6 eV interact with the aerosol particles. The photoelectron spectra thus obtained at a few altitudes are presented in Figure 9 and the integrated photoelectron production rate as a function of altitude is presented in Figure 10. It is evident from Figure 10 that the photoelectron production peaks at the surface of Mars.

6. Attachment Coefficients

[18] There are three types of theories for ion-aerosol attachment [*Yair and Levin*, 1989]. Ion diffusion to surface of particles occurs when the radii of particles are larger than

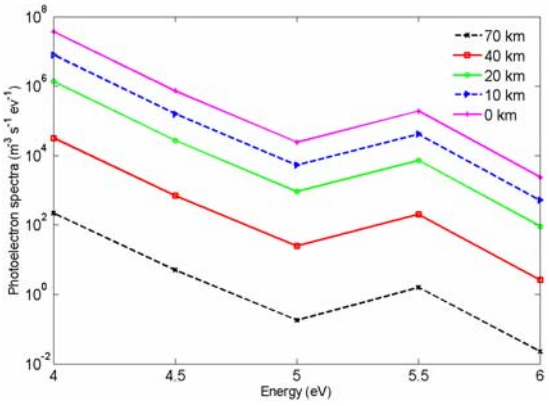

Figure 9. Photoelectron flux at different altitudes in the atmosphere.

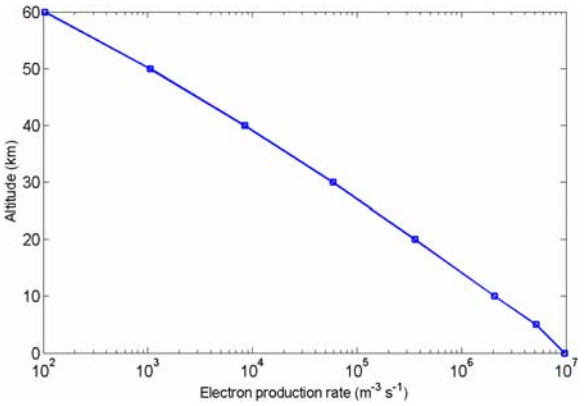

Figure 10. Photoelectron production rate.

the ionic mean free path. Here ions are trapped by image force. Free molecular theory uses a kinetic approach when the radii of particles are much smaller than the ionic mean free path. Here the attachment occurs via 3-body collision (similar to the ion-ion recombination). Transition regime theory is used when the size of the particles and the ionic mean free path become comparable. In this regime a combination of the above two mechanisms are used. The ionic mean free path can be written in terms of the mobility and ionic mass by means of the equation

$$K = 0.75\frac{e\lambda}{M\overline{\nu}}\left(1+\frac{M}{m}\right)^{1/2} \tag{4}$$

where λ is the mean free path, K is the ionic mobility, m is the mass of the ion, M is the mass of the gas (CO_2) and $\overline{\nu}$ is the average thermal velocity. The ionic mobility is calculated as [*Borucki et al.*, 1982],

$$K = 3.74\times10^{20}(\mu\xi)^{-1/2}n^{-1} \tag{5}$$

where μ is the reduced mass of the ion-gas system, ξ is the polarizability of CO_2, and n is the number density of CO_2. The value of ξ is 2.6 Å^3 [*Borucki et al.*, 1982].

[19] As the Martian atmosphere is tenuous, the ionic mean free path is comparable to the size of the aerosols close to the surface and is larger than the size of the aerosols at higher altitudes. Therefore free molecular theories and transition theories prevail in the lower atmosphere. A direct comparison of the size of the particles and the mean free path is provided by *Michael and Tripathi* [2008].

[20] The theory of the diffusion of ions to aerosols with radii larger than the ionic mean free path is well established. The study of the attachment of ion to aerosols of radii comparable to or smaller than the ionic mean free path has been more difficult [*Hoppel and Frick*, 1986]. The concept of the limiting sphere, which is concentric with the aerosol but with radius the order of one mean free path larger than the aerosol, was defined by *Fuchs* [1964]. The diffusion mobility treatment hold outside this sphere and kinetic theory is applied inside.

[21] If the aerosol carries a single charge then the ion-aerosol recombination coefficient reduces to the ion-ion recombination coefficient and can be explained using 3-body trapping theory, which requires the trapping distance. Three-body recombination was originally developed to describe ion-ion recombination. When two ions approach one another the relative kinetic energy increases at the expense of the potential energy. If one of the ions experiences a thermalizing collision with a third body while in the vicinity of the other ion, then the relative kinetic energy is reduced. If such a thermalizing collision occurs within a certain minimum separation distance between the ions, the total relative energy of the ion pair can be reduced and the ions will then move in bound trajectories about one another and recombination will result. *Natanson* [1960] used the same theory for the ion-aerosol attachment when the size of the particle is very small, which is the case for the tenuous atmosphere of Mars.

[22] Ion-aerosol trapping distance is obtainable from the ion-ion trapping distance, which can be calculated from the ion-ion recombination coefficient [*Natanson*, 1960]. In addition to the 3-body trapping there can be trapping of the ion by image force (forces which increase faster than the inverse square law). Image force can lead to orbits which spiral into the aerosol, which means any ion which approach the aerosol closer than the image capture distance will spiral into the aerosol under the influence of the image force. *Jensen and Thomas* [1991] used the expression developed by *Natanson* [1960] to calculate the ion capture rates by small ice and meteoric particles in the mesosphere of Earth's atmosphere.

[23] *Hoppel and Frick* [1986] estimated the relative importance of image capture and three-body trapping and both effects are included in a single theory to calculate the attachment coefficients. Figure 11 demonstrates the two trapping spheres. The image capture sphere is defined by the distance (Δ) which is the minimum apsidal distance. Minimum apsidal distance is the distance of closest approach where radial velocity vanishes. If the impact parameter is greater than b_Δ the ion escapes, and if the impact parameter is less than b_Δ the ion spirals into the aerosol.

[24] When an ion collides with an aerosol, part of its kinetic energy is removed by the aerosol. If this energy is sufficiently high the ion will be trapped in the coulomb field of the aerosol. The 3-body trapping distance δ is defined as the average separation distance where the removed energy is enough to ensure trapping. If the image capture distance Δ is greater than the three body trapping distance δ, then three body trapping is not important. Δ is always larger than δ for

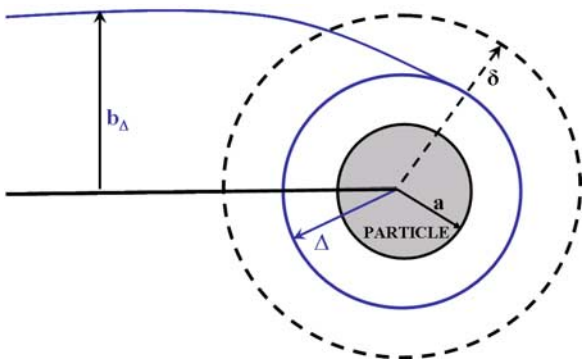

Figure 11. Schematic of the image capture and 3-body trapping distances.

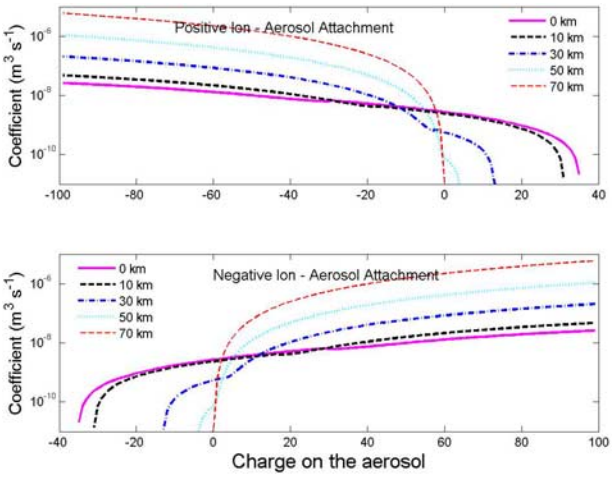

Figure 12. Ion-aerosol attachment coefficient at various altitudes.

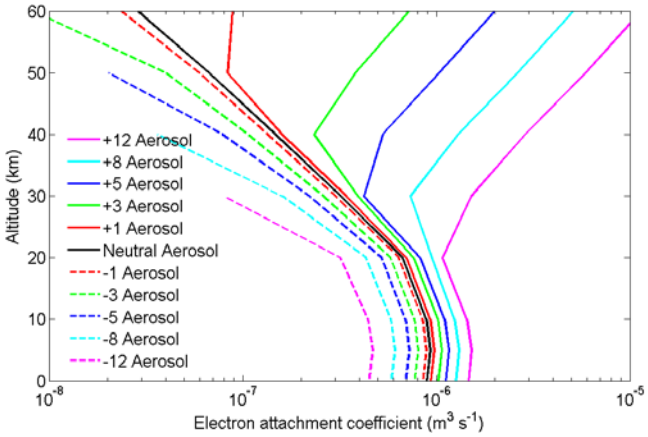

Figure 13. Altitude profile of electron-aerosol attachment coefficient.

uncharged aerosol. However if the ion and the aerosol have opposite polarity, there is a critical radius of the aerosol below which the 3-body trapping becomes important. If the ion is more than one mean free path from the larger of Δ or δ, then the diffusion mobility equation is assumed to hold.

[25] In the present work the method developed by *Hoppel and Frick* [1986] is used to calculate the attachment coefficients of ions to the aerosols. For more details of the calculations the reader is referred to *Tripathi and Michael* [2008] and *Tripathi et al.* [2008]. The ion-aerosol attachment coefficients for positively and negatively charged ions with aerosols charged from −100 to +100 is calculated and presented in Figure 12. It is apparent from Figure 12 that the attachment coefficients of positive ions with positively charged particles decreases as the charge on the particle increases and vice versa. Similarly, attachment coefficients of negative ions with negatively charged particles decrease as the charge on the particle increases and vice versa.

[26] According to *Gunn* [1954] the electron-aerosol attachment coefficient can be calculated using the formula,

$$\beta_e = \frac{4\pi p K_e}{1 - \exp(-pe/akT)} \tag{6}$$

where a is the radius of the aerosol, p is the average number of elementary charges, e is the electron charge, k is the Boltzmann constant and T is the temperature. Here K_e is the electron mobility which is calculated using the following equation [*Borucki et al.*, 1982].

$$K_e = e/\nu m_e \tag{7}$$

where m_e is the mass of the electron and ν is the momentum transfer collision frequency of electrons in CO_2, which is about 1.0×10^{-7} n s^{-1}, where n is the number density of CO_2. The altitude profile of the electron attachment coefficient is presented in Figure 13. It is evident from the figure that the attachment coefficients to negatively charged aerosols decreases as the charge on the aerosol increases and the attachment coefficient increases as the positive charge on the particle increases. As it is a function of mobility (which increases as altitude increases) and aerosol size (which decreases as altitude increases) the attachment coefficients initially decrease with altitude and then become saturated or slowly increase.

7. Day-Time Calculations

[27] The flow diagram of the charging calculations is presented in Figure 14. Concentrations of ions, electrons and aerosols can be found from the three-level probabilistic master equations. These constitute a set of 2p + 4 simultaneous differential equations, p being the maximum number of elementary charges allowed on a particle [*Yair and Levin*, 1989]. For the day time calculations a new equation for electron concentration has been added to the set of equations for the nighttime calculations which are presented by *Michael et al.* [2007]. The production terms in this equation are the electron production rate and the electron detachment from negative ions. The loss terms are the electron-positive ion recombination and attachment of electrons to the aerosols. The additional term of electron-positive ion recombination appears in the equation for the concentration of positive ions. The maximum charge an aerosol can attain is assumed as ±100 [*Michael et al.*, 2007] and therefore there are 201 equations for the neutral and charged aerosol concentrations. For the day-time calculation there are two additional terms of electron attachment to aero-

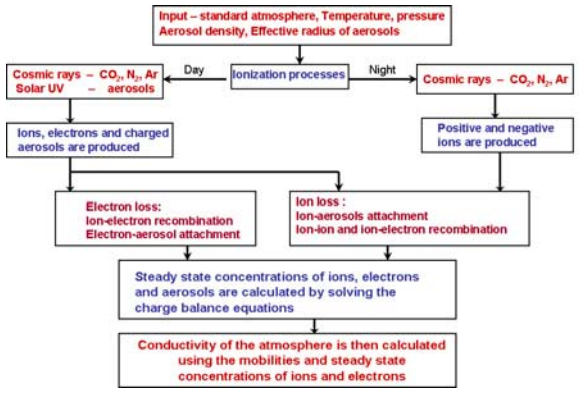

Figure 14. Schematic of the aerosol charging calculation.

sols in each of the 201 equations for the nighttime aerosol concentrations.

[28] The ion and electron charge balance equations can thus be written as

$$\frac{dn^+}{dt} = q_{ion} - \alpha n^+ n^- - \alpha_e n^+ n^e - \sum_i \left(\beta_1^{(i)} n^+ N^i\right) \quad (8)$$

$$\frac{dn^-}{dt} = q_{ion} - \alpha n^+ n^- - \sum_i \left(\beta_2^{(i)} n^- N^i\right) - F n^- \quad (9)$$

$$\frac{dn^e}{dt} = q_e - \alpha_e n^+ n^e - \sum_i \left(\beta_e^{(i)} n^e N^i\right) + F n^- \quad (10)$$

Here, α is the ion-ion recombination coefficient, α_e is the electron-ion recombination coefficient, q_{ion} is the ion production rate, q_e is the electron production rate, β_j^i is the attachment coefficient for ions of polarity j (1 for positive and 2 for negative) to particles with charge i, β_e^i is the electron attachment coefficient to particles with charge i, and N^i is the density of particles of charge i. F represents the detachment of electrons from negative ions. F is evaluated using the equation from *Borucki et al.* [1982].

$$F \approx p\pi^{1/2} \frac{L_m}{L_I} \frac{P}{KT} \sigma^2 \left(\frac{8KT}{\pi m}\right)^{1/2} \left(\frac{E_a}{KT} + 1\right) \exp\left(-\frac{E_a}{KT}\right) \quad (11)$$

Here p is the probability of an energetic collision removing an electron ($\sim$0.02), L_M/L_I is the ratio of the mean free path of neutral molecules to that of ions, P is the pressure, σ is the collision cross section ($\sim 10^{-8}$ cm^2), E_a is the electron affinity of the negative ions ($\sim$2 eV), m is the mass of the negative ions, k is the Boltzmann constant, and T is the temperature. F was estimated and found that in the atmosphere of Mars it is negligible. *Borucki et al.* [1982] calculated the value of F in the atmosphere of Venus and found that the electron concentration would be significantly affected by electron detachment only when F is at least 10% of the ionization rate and is important only near the surface. As the atmospheric pressure of Mars is much lower than that at Venus, F becomes negligible in the atmosphere of Mars.

[29] *Parthasarathty* [1976] derived a steady state recurrence relation to compute the build-up of electric charge on aerosol particles due to collision with positive and negative ions and electrons. *Whitten et al.* [2007] modified the recurrence expression given by *Parthasarathty* [1976] to reflect the time dependence of the charge accumulation by aerosols. The time dependent charge balance equations for the aerosols can be written as

$$\frac{dN^i}{dt} = \beta_1^{(i-1)} n^+ N^{(i-1)} + \beta_2^{(i+1)} n^- N^{(i+1)} + \beta_e n^e N^{(i+1)} - \beta_1^{(i)} n^+ N^i - \beta_2^{(i)} n^- N^i - \beta_e n^e N^i \quad (12)$$

Here βe is the electron-aerosol attachment coefficient. Since the elementary charges on the aerosols are allowed to vary between plus and minus 100, there are 204 simultaneous differential equations for each altitude. The differential equations are solved using the 4th order Runge-Kutta method. Runge-Kutta methods are an important family of iterative methods for the approximation of solutions of ordinary differential equations. This method numerically integrates ordinary differential equations by using a trial step at the midpoint of an interval to cancel out lower-order error terms. This approach is used to solve the set of equations at every 10 km altitude intervals using the charge conservation as a constraint on the calculations. This requirement that every volume of space be electrically neutral entails the following condition.

$$zp + n^+ - n^- - n^e = 0 \quad (13)$$

Here n^+, n^- and n^e are the positive, negative and electrons densities, respectively and zp is the total charge on the aerosols which is expressed as,

$$zp = \sum_p p N_p \quad (14)$$

where N_p is the density of aerosols with charge state p.

[30] After the steady state is achieved, the conductivity of the atmosphere is calculated as

$$\sigma = e(n_+ K_+ + n_- K_- + n_e K_e) \quad (15)$$

where, e is the electronic charge, n and n_e are the number densities of ions and electrons and K and K_e are the corresponding mobilities. The ionic mobility is calculated using equation (5) and the electron mobility is calculated using equation (7).

8. Results and Discussion

[31] GCR are the only source of ionization at night and both positive and negative ion clusters are considered for aerosol charging at night [*Michael et al.*, 2007]. Therefore there were charge balance equations for positive and negative ions and neutral and charged aerosols. During the day-time, besides cosmic rays, there are solar photons which knock out electrons from aerosols. Therefore a charge balance equation for electrons is also included for the day-time study. Equations (8), (9), (10) and (12) were solved to find the steady state concentrations of ions, electrons and neutral and charged aerosols. The positive and negative ionic concentrations were considered equal, $(q/\alpha)^{0.5}$, initially. As the electrons are produced from aerosols the initial concentration of electrons is considered $(q_e/\beta_e)^{0.5}$. The initial charged aerosol densities are estimated in such a way that the condition of electrical neutrality is preserved. The ion production from GCR corresponds to that of the solar minimum conditions, so that the GCR flux and the ion production are the maximum. The aerosol concentration and effective radius correspond to the variance of 0.25. The atmospheric density and temperature are taken from *Magalhaes et al.* [1999].

[32] Figure 15a presents the probability of particles to acquire charges at 0 km for the day and nighttime atmosphere. Apparently the charge distribution peaks at 9 negative charge at altitude 0 km during the day-time and

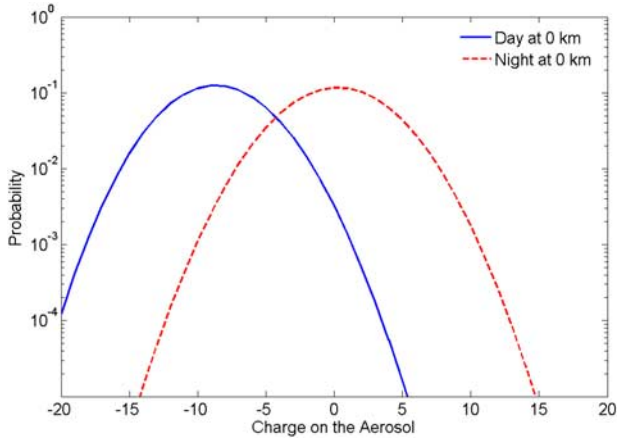

Figure 15a. Probability of charge distribution on aerosols at 0 km for the day and nighttime.

the aerosols are symmetrically charged during the nighttime. Close to the surface there are more negatively charged aerosols as the electron density is higher. The charge distribution at altitudes 0, 10, 20, and 50 are presented in Figure 15b. As solar UV radiation removes electrons from aerosols, there is a charge distribution of aerosols at the beginning of the calculation, which is generated using equation (13). Since the mobility of electrons is about 3 orders of magnitude larger than that of the positive ions, there are more negatively charged particles at 0 km. At higher altitudes the aerosol charge distributions become symmetric as the electron contribution is very small at those altitudes. Though the electron attachment coefficient increases at higher altitudes, the electron concentration becomes very small to entail an effect on aerosol charging. For a direct comparison, the charge distribution of aerosols during the nighttime at similar altitudes are presented in Figure 15c. During the nighttime there are only positive and negative ions and no electrons. The ions have similar mobility and attachment coefficients and therefore the aerosols are almost symmetrically charged as depicted in Figure 15c.

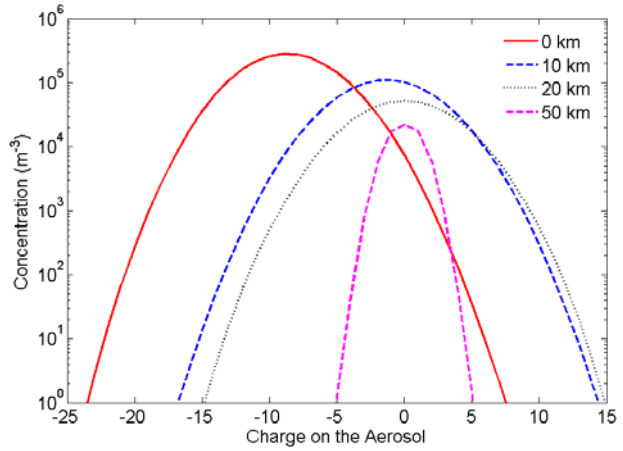

Figure 15b. Steady state charged aerosol concentration as a function of charge for the day-time.

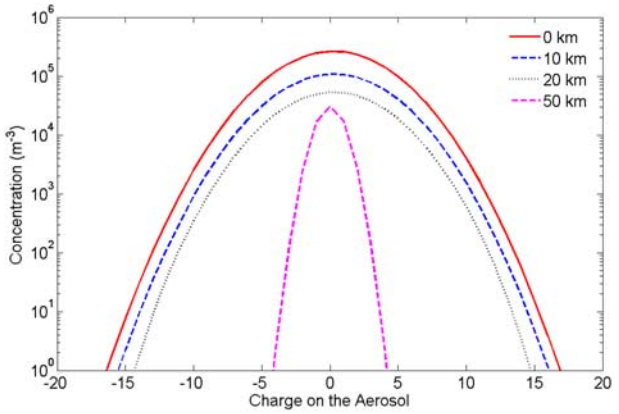

Figure 15c. Steady state charged aerosol concentration as a function of charge for the nighttime.

[33] Steady state ion and electron concentrations are presented in Figure 16. The initial concentrations of ions and electrons are also shown in Figure 16 for comparison. It is evident that more than 60% of the ions get attached to aerosols that are close to the surface and most of the ion-aerosol attachment occurs at altitudes less than 30 km. More than 95% of the electrons get attached to aerosols close to the surface. Though the electron concentration is less than the ion concentration by more than 2 orders of magnitude, the mobility and the electron attachment coefficients are about 3 orders of magnitude higher than those of ions. Therefore the electron attachment to the aerosols does make an impact on the aerosol charging.

[34] When the steady state is achieved the conductivity of the atmosphere is calculated. The atmospheric conductivity can be expressed in terms of the number densities and mobilities of the individual charged species as expressed in equation (15). The attachment of ions and electrons to aerosols reduces the conductivity as they become almost immobile. The calculated atmospheric conductivity is presented in Figure 17 in the presence (solid line with squares) and absence (solids line with circles) aerosols It is evident that the conductivity of the atmosphere is reduced by a factor of 2 at the surface for the day-time atmosphere of Mars. The atmospheric conductivity with and without

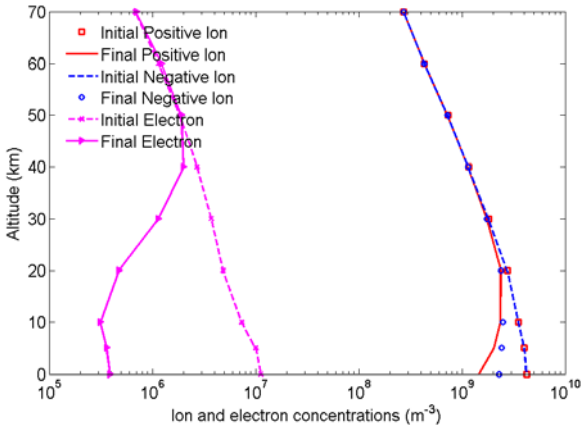

Figure 16. Initial and final ion and electron concentration for the day-time.

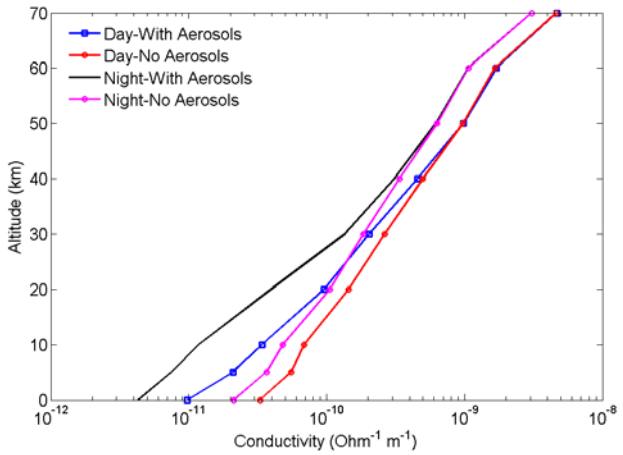

Figure 17. Conductivity of the atmosphere for the day and nighttime.

aerosols for the nighttime is also presented in Figure 17 for direct comparison.

[35] *Bertherlier et al.* [2000] and *Grard* [1995] suggested that the best estimate of the conductivity at the surface is in the range $\sim 10^{-12}$–10^{-10} Ohm^{-1} m^{-1}. In the present work the electrical conductivity of the atmosphere was found to be 1×10^{-11} Ohm^{-1} m^{-1} at the surface, which is within the predicted range. The variation in conductivity corresponding to different aerosol characteristics, opacities, solar conditions and temperature are discussed by *Michael et al.* [2007]. The effect of dust storms on the atmospheric conductivity is illustrated by *Michael and Tripathi* [2008].

9. Summary

[36] The charging of aerosols and the conductivity of the day-time lower atmosphere of Mars has been calculated. The study of atmospheric conductivity is very important in understanding the global electric circuit of the Martian atmosphere. Galactic cosmic rays are the major atmospheric ionization agent for both the day and nighttime atmosphere. In addition, solar UV photons of energy less than 6 eV can reach the lower atmosphere. These photons interact strongly with aerosols producing photoelectrons. Therefore molecular ions and electrons contribute to the conductivity of the day-time atmosphere. Ion and electron attachment rates to aerosols have been estimated for the altitude range (0–70 km) considered. Coupled charge balance equations for ions, electrons and aerosols have been solved to find the steady state concentrations. There are more negatively charged aerosols than positively charged aerosols in steady state close to the surface due to the efficient attachment of electrons to the aerosols. The steady state concentrations of ions and electrons were then used to calculate the conductivity of the atmosphere. The presence of free electrons increases the atmospheric conductivity by a factor of about 2.5 at the surface.

[37] **Acknowledgments.** The authors acknowledge the support of the Indian Space Research Organisation Planex program. The authors also gratefully acknowledge Karen O'Brien for providing the ionization rate profiles.

References

Banks, P. M., and G. Kockarts (1973), *Aeronomy*, pp. 257–260 Part B. Academic Press, New York.
Bertherlier, J. J., R. Grard, H. Laakso, and M. Parrot (2000), ARES atmospheric relaxation and electric field sensor, the electric field experiment on NETLANDER, *Planet. Space Sci.*, *48*, 1183–1200.
Boella, G., C. Dilworth, M. Panetti, and L. Scarsi (1968), The atmospheric and leakage flux of neutrons produced in the atmosphere by cosmic ray interactions, *Earth Planet. Sci. Lett.*, *4*, 393–398.
Borucki, W. J., Z. Levin, R. C. Whitten, R. G. Keesee, L. A. Capone, O. B. Toon, and J. Dubach (1982), Predicted electrical conductivity between 0 and 80 km in the Venusian atmosphere, *Icarus*, *51*, 302–321.
Borucki, W. J., R. C. Whitten, E. L. O. Bakes, E. Barth, and S. N. Tripathi (2006), Predictions of the electrical conductivity and charging of the aerosols in Titan's atmosphere 6/20/05, *Icarus*, *181*, 527–544.
Chassefiere, E., J. E. Blamont, V. A. Krasopolsky, O. I. Korablev, S. K. Atreya, and R. A. West (1992), Vertical structure and size distributions of Martial aerosols from solar occultation measurements, *Icarus*, *97*, 46–69.
Chassefiere, E., P. Drossart, and O. Korablev (1995), Post-Phobos model for the altitude and size distribution of dust in the low Martian atmosphere, *J. Geophys. Res.*, *100*(E3), 5525–5539.
Clancy, R. T., and S. W. Lee (1991), A new look at dust and clouds in the Mars atmosphere: Analysis of emission-phase function sequences from global Viking IRTM observations, *Icarus*, *93*, 135–158.
Clancy, R. T., M. J. Wolff, and P. R. Christensen (2003), Mars aerosol studies with the MGS TES emission phase function observations: Optical depths, particle sizes, and ice cloud types versus latitude and solar longitude, *J. Geophys. Res.*, *108*(E9), 5098, doi:10.1029/2003JE002058.
Conrath, B. J. (1975), Thermal structure of the Marian atmosphere during the dissipation of the dust storm of 1971, *Icaurs*, *24*, 36–46.
Dave, J. V. (1968), "Subroutines for Computing the Parameters of the Electromagnetic Radiation Scattered by Spheres", Report No. 320–3237, available from IBM Palo Alto Scientific Center, 1530 Page Mill Road Palo Alto, California 94304, USA.
Drossart, P., J. Rosenqvist, S. Erard, Y. Langevin, J. P. Bibring, and M. Combes (1991), Martian aerosol properties from the Phobos/ISM expt, *Ann. Geophys.*, *9*, 754–760.
Farrell, W. M., and M. D. Desch (2001), Is there a Martian atmospheric electric circuit, *J. Geophys. Res.*, *106*(E4), 7591–7595.
Farrell, W. M., M. L. Kaiser, M. D. Desch, J. G. Houser, S. A. Cummer, D. M. Wilt, and G. A. Landis (1999), Detecting electrical activity from Martian dust storms, *J. Geophys. Res.*, *104*(E2), 3795–3801.
Ferguson, D. C., L. C. Kolecki, M. W. Siebert, D. M. Wilt, and J. R. Matijevic (1999), Evidence from Martian electrostatic charging and abrasive wear from the Wheel Abrasion Experiment on the Pathfinder Sojourner rover, *J. Geophys. Res.*, *104*(E4), 8747–8759.
Fuchs, N. A. (1964), On the steady-state charge distribution on aerosol particles in a bipolar ionized atmosphere, *Izv. Geophys. Ser.*, *4*, 579–586.
Grard, R. (1995), Solar photon interaction with the Martian surface and related electrical and chemical phenomena, *Icarus*, *114*, 130–138.
Gunn, R. (1954), Diffusion charging of atmospheric droplets by ions and the resulting combination coefficients, *J. Meteorol.*, *11*, 339–347.
Hinson, D. P., M. D. Smith, and B. J. Conrath (2004), Comparison of atmospheric temperatures obtained through infrared sounding and radio occultation by Mars Global Surveyor, *J. Geophys. Res.*, *109*, E12002, doi:10.1029/2004JE002344.
Hoppel, W. A., and G. M. Frick (1986), Ion-aerosol attachment coefficients and the steady-state charge on aerosols in a bipolar ion environment, *Aerosol Sci. Technol.*, *5*, 1–21.
Jensen, E. J., and G. E. Thomas (1991), Charging of mesospheric particles: Implications for electron density and particle coagulation, *J. Geophys. Res.*, *96*(D10), 18,603–18,615.
Kerzhanovich, V. V. (1977), Mars 6: Improved analysis of the descent module measurements, *Icarus*, *30*, 1–25.
Korablev, O. I., V. A. Krasopolsky, A. V. Rodin, and E. Chassefiere (1993), Vertical structure of the Martian dust measured by the solar infrared occultations from the Phobos spacecraft, *Icarus*, *102*, 76–87.
Krauss, C. E., M. Horanyi, and S. Robertson (2006), Modeling the formation of electrostatic discharges on Mars, *J. Geophys. Res.*, *111*, E02001, doi:10.1029/2004JE002313.
Kuhn, W. R., and S. K. Atreya (1979), Solar radiation incident on the Martian surface, *J. Mol. Evol.*, *14*, 57–64.
Magalhaes, J. A., J. T. Schofield, and A. Seiff (1999), Results of the Mars Pathfinder atmospheric structure investigation, *J. Geophys. Res.*, *104*, 8943–8955.
Melnik, O., and M. Parrot (1998), Electrostatic discharge in Martian dust storms, *J. Geophys. Res.*, *103*(A12), 29,107–29,117.
Michael, M., and S. N. Tripathi (2008), Effect of charging of aerosols in the lower atmosphere of mars during the dust storm of 2001, *Planet. Space Sci.*, in press.

Michael, M., M. Barani, and S. N. Tripathi (2007), Numerical predictions of aerosol charging and electrical conductivity of the lower atmosphere of Mars, *Geophys. Res. Lett.*, *34*, L04201, doi:10.1029/2006GL028434.

Molina-Cuberos, G. J., J. J. Lopez-Moreno, R. Rodrigo, L. M. Lara, and K. O'Brien (1999), Ionization by cosmic rays of the atmosphere of Titan, *Planet Space Sci.*, *47*, 1347.

Molina-Cuberos, G. J., J. J. Lopez-Moreno, R. Rodrigo, H. Lichtenegger, and K. Schwingenschuh (2001), A model of the Martian ionosphere below 70 km, *Adv. Space Res.*, *27*, 1801–1806.

Montmessin, F., E. Qu'emerais, J. L. Bertaux, O. Korablev, P. Rannou, and S. Lebonnois (2006), Stellar occultations at UV wavelengths by the SPICAM instrument: Retrieval and analysis of Martian haze profiles, *J. Geophys. Res.*, *111*, E09S09, doi:10.1029/2005JE002662.

Murphy, J. R., R. M. Haberle, O. B. Toon, and J. B. Pollack (1993), Martian global dust storms - Zonally symmetric numerical simulations including size-dependent particle transport, *J. Geophys. Res.*, *98*(E2), 3197–3220.

Natanson, G. L. (1960), On the theory of charging of microscopic aerosol particles resulting from the capture of gas ions, *Zh. Technol. Fiz.*, *30*, 573–588.

O'Brien, K. (1970), Calculated cosmic ray ionization in the lower ionosphere, *J. Geophys. Res.*, *75*(22), 4357–4359.

Pang, K., and J. M. Ajello (1977), Complex refractive index of Martian dust - Wavelength dependence and composition, *Icarus*, *30*, 63–74.

Parthasarathty, R. (1976), Mesopause dust as a sink for ionization, *J. Geophys. Res.*, *81*(13), 2392–2396.

Pollack, J. B., D. S. Colburn, F. M. Flasar, R. Kahn, C. E. Carlston, and D. G. Pidek (1979), Properties and effects of dust particles suspended in the Martian atmosphere, *J. Geophys. Res.*, *84*(B6), 2929–2945.

Read, P. L., and S. R. Lewis (2004), Dust storms, devils, and transport, in *The Martian Climate Revisited*, pp. 179–217, Springer, Chichester, UK.

Roesler, S., W. Heinrich, and H. Schraube (1998), Neutron spectra in the atmosphere from interactions of primary cosmic rays, *Adv. Space Res.*, *21*, 1717–1726.

Seiff, A. (1976), The Viking atmosphere structure experiment—Techniques, instruments, and expected accuracies, *Space Sci. Instrum.*, *2*, 381–423.

Seiff, A., and D. B. Kirk (1977), Structure of the atmosphere of Mars in summer at midlatitudes, *J. Geophys. Res.*, *82*, 4364–4378.

Toon, O. B., J. B. Pollack, and C. Sagan (1977), Physical properties of the particles composing the Martian dust storm of 1971–1972, *Icarus*, *30*, 663–696.

Tripathi, S. N., and M. Michael (2008), Aerosols in the atmosphere of Mars, in *Chapter 3, Modeling of Planetary Atmosphere*, edited by S. A. Haider, V. Sheel, and S. Lal, Mcmillan, India.

Tripathi, S. N., M. Michael, and R. G. Harrison (2008), Profiles of ion and aerosol interactions in planetary atmospheres, *Space Sci. Rev.*, doi:10.1007/s11214-008-9367-7.

Whitten, R. C., I. G. Poppoff, and J. S. Sims (1971), The ionosphere of mars below 80 km altitude—I quiescent conditions, *Planet. Space Sci.*, *17*, 243–250.

Whitten, R. C., W. J. Borucki, and S. N. Tripathi (2007), Predictions of the electrical conductivity and charging of the aerosols in Titan's nighttime atmosphere, *J. Geophys. Res.*, *112*, E04001, doi:10.1029/2006JE002788.

Whitten, R. C., W. J. Borucki, and S. N. Tripathi (2008), Predictions of the electrical conductivity and charging of the cloud particles in Jupiter's atmosphere, *J. Geophys. Res.*, *113*, E04001, doi:10.1029/2007JE002975.

Yair, Y., and Z. Levin (1989), Charging of polydispersed aerosol particles by attachment of atmospheric ions, *J. Geophys. Res.*, *94*(D11), 13,085–13,091.

M. Michael, S. K. Mishra, and S. N. Tripathi, Department of Civil Engineering, Indian Institute of Technology, Kanpur-208016, UP, India. (snt@iitk.ac.in)